Constraints on the sources of tropospheric ozone from ^{210}Pb-^{7}Be-O_3 correlations

Hongyu Liu[1] and Daniel J. Jacob

Department of Earth and Planetary Sciences and Division of Engineering and Applied Sciences, Harvard University, Cambridge, Massachusetts, USA

Jack E. Dibb

Institute for the Study of Earth, Oceans and Space, University of New Hampshire, Durham, New Hampshire, USA

Arlene M. Fiore[2] and Robert M. Yantosca

Department of Earth and Planetary Sciences and Division of Engineering and Applied Sciences, Harvard University, Cambridge, Massachusetts, USA

Received 18 July 2003; revised 22 December 2003; accepted 12 February 2004; published 10 April 2004.

[1] The ^{210}Pb-^{7}Be-O_3 relationships observed in three aircraft missions over the western Pacific (PEM-West A and B, TRACE-P) are simulated with a global three-dimensional chemical tracer model (GEOS-CHEM) driven by assimilated meteorological observations. Results are interpreted in terms of the constraints that they offer on sources of tropospheric ozone (O_3). Aircraft observations of fresh Asian outflow show strong ^{210}Pb-O_3 correlations in September–October, but such correlations are only seen at low latitudes in February–March. Observations further downwind over the Pacific show stronger ^{210}Pb-O_3 correlations in February–March than in September–October. The model reproduces these results and attributes the seasonal contrast to strong O_3 production and vertical mixing over east Asia in September–October, seasonal shift of convection from China in September–October to Southeast Asia in February–March, and slow but sustained net O_3 production in Asian outflow over the western Pacific in February–March. Seasonal biomass burning over Southeast Asia in February–March is responsible for the positive ^{210}Pb-O_3 correlations observed at low latitudes. The model reproduces the observed absence of ^{7}Be-O_3 correlations over the western Pacific during September–October, implying strong convective and weak stratospheric influence on O_3. Comparison of observed and simulated ^{7}Be-O_3 correlations indicates that the stratosphere contributes less than 20–30% of O_3 in the middle troposphere at northern midlatitudes even during spring. *INDEX TERMS:* 0368 Atmospheric Composition and Structure: Troposphere—constituent transport and chemistry; 0365 Atmospheric Composition and Structure: Troposphere—composition and chemistry; 0345 Atmospheric Composition and Structure: Pollution—urban and regional (0305); *KEYWORDS:* lead-210 and beryllium-7, Asian outflow of ozone, biomass burning, stratosphere-troposphere exchange

Citation: Liu, H., D. J. Jacob, J. E. Dibb, A. M. Fiore, and R. M. Yantosca (2004), Constraints on the sources of tropospheric ozone from ^{210}Pb-^{7}Be-O_3 correlations, *J. Geophys. Res.*, *109*, D07306, doi:10.1029/2003JD003988.

1. Introduction

[2] Understanding the factors controlling tropospheric ozone (O_3) is a central issue in tropospheric chemistry. Tropospheric O_3 is a greenhouse gas, a surface air pollutant, and a key player in controlling the oxidizing power of the atmosphere [*Thompson*, 1992]. Industrialization of the Asian continent is expected to be the principal driver of global change in atmospheric composition over the next decades [*Ehhalt and Prather*, 2001]. Better understanding of the Asian source of O_3 and its global impact is essential. We recently quantified the sources contributing to tropospheric O_3 over the Asian Pacific Rim in different seasons through a global three-dimensional (3-D) model analysis of Hong Kong and Japanese ozonesonde observations [*Liu et al.*, 2002]. In this paper, we apply the same model to examine the constraints offered by aircraft observations of ^{210}Pb-^{7}Be-O_3 correlations in Asian outflow over the western Pacific.

[3] Lead-210 (half-life 22 years) is the decay daughter of ^{222}Rn (half-life 3.8 days) which is emitted from soils by decay of ^{226}Ra [*Turekian et al.*, 1977]. Beryllium-7 (half-life 53.3 days) is produced by cosmic ray spallation reactions with nitrogen and oxygen in the stratosphere and

[1] Also at National Institute of Aerospace, Hampton, Virginia, USA.

[2] Now at Program of Atmospheric and Oceanic Sciences, Princeton University, Princeton, New Jersey, USA.

0148-0227/04/2003JD003988$09.00

upper troposphere. Both ^{210}Pb and ^{7}Be attach to aerosols following production, and are principally removed by precipitation scavenging. Lead-210 is a tracer of continental influence [*Balkanski et al.*, 1993], while ^{7}Be is a tracer of stratospheric influence [*Viezee and Singh*, 1980; *Dibb et al.*, 1992, 1994] and subsidence [*Feely et al.*, 1989; *Koch et al.*, 1996]. One may therefore expect ^{210}Pb-^{7}Be-O_3 correlations to provide information on the origin of O_3. Strong correlations of O_3 with ^{7}Be observed at surface and mountain sites have been interpreted in a number of studies as evidence for a stratospheric or upper tropospheric source of O_3 [*Johnson and Viezee*, 1981; *Reiter et al.*, 1983; *Prospero et al.*, 1995; *Moody et al.*, 1995; *Tsutsumi et al.*, 1998]. A recent global 3-D model analysis suggests that there are confounding factors in this interpretation [*Li et al.*, 2002a].

[4] Aircraft observations of ^{210}Pb and ^{7}Be up to 12-km altitude have been made by J. E. Dibb on a number of atmospheric chemistry field campaigns over the past decade. Detection limits for 10–30 min samples are 0.5 femtocurie per standard cubic meter (fCi SCM^{-1}) for ^{210}Pb, and 10 fCi SCM^{-1} for ^{7}Be, sufficiently low to provide valuable data throughout the troposphere. We focus our attention on three campaigns (PEM-West A and B, TRACE-P) for which the data sets are particularly extensive and aimed at characterization of Asian outflow (Figure 1). The data reveal perplexing ^{210}Pb-^{7}Be-O_3 correlations [*Dibb et al.*, 1996, 1997, 2003] that provide as we will see important constraints on the sources of tropospheric O_3 and the role of Asian outflow.

[5] Our analysis will be based on the GEOS-CHEM global 3-D model of tropospheric chemistry [*Bey et al.*, 2001a] driven by assimilated meteorological observations from the Goddard Earth Observing System data assimilation system (GEOS DAS) at the NASA Global Modeling and Assimilation Office (GMAO). The GEOS-CHEM model has been used extensively for simulations of tropospheric O_3, as reviewed in the next section, and has also been used for global simulation of ^{210}Pb and ^{7}Be [*Liu et al.*, 2001]. It was recently applied to interpret observed ^{210}Pb-^{7}Be-O_3 correlations at two North Atlantic surface sites [*Li et al.*, 2002a].

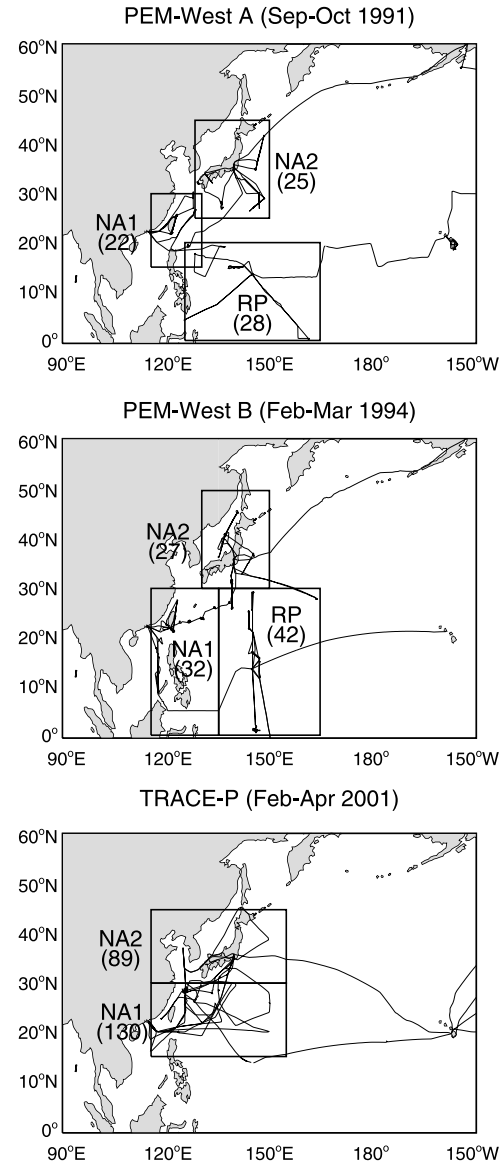

Figure 1. Aircraft (DC-8) flight tracks from three aircraft missions where concurrent measurements of O_3, ^{210}Pb, and ^{7}Be concentrations are available. The missions are the Pacific Exploratory Mission over the western North Pacific phase A (PEM-West A, September–October 1991) [*Hoell et al.*, 1996], PEM-West B (February–March 1994) [*Hoell et al.*, 1997], and the Transport and Chemical Evolution over the Pacific mission (TRACE-P, February–April 2001) [*Jacob et al.*, 2003]. The squares are coherent regions for data analysis similar to those previously identified by *Dibb et al.* [1996, 1997, 2003]: remote Pacific (RP) and near Asia (NA1 and NA2). The number of observations of ^{210}Pb and ^{7}Be for each region is also shown.

2. Model Simulations

[6] Global simulations were conducted for the years 1991, 1994, and 2001 using GEOS-CHEM version 4.6 for 1991 and 1994, and version 4.26 for 2001 (see http://www-as.harvard.edu/chemistry/trop/geos). The GEOS data are from the GEOS1 assimilation for 1991 and 1994 (2° × 2.5° horizontal resolution, 20 sigma vertical levels), and GEOS3 for 2001 (1° × 1°, 48 levels). The horizontal resolution is degraded here to 4° × 5° for computational expediency. The model uses the advection scheme of *Lin and Rood* [1996] and the moist convective mixing scheme of *Allen et al.* [1996]. We assume complete vertical mixing within the GEOS-diagnosed mixed layer. Chemical tracer evaluations of convective transport in the GEOS fields have been presented by *Allen et al.* [1996], *Liu et al.* [2001], and *Bell et al.* [2002].

[7] *Liu et al.* [2001] presented a detailed description of the simulation capability for ^{210}Pb and ^{7}Be in GEOS-CHEM. Simulation of aerosol wet deposition includes scavenging in wet convective updrafts (with midlevel entrainment and detrainment), and first-order rainout and washout from both convective and large-scale precipitation. Return to the atmosphere following evaporation of precipitation is allowed. There is also a small dry deposition sink represented with a resistance-in-series model [*Wesely and Hicks*, 1977]. Cirrus precipitation not accounted for in the

assimilated meteorological data [*Lawrence and Crutzen*, 1998] improves some aspects of the ^{210}Pb-^{7}Be simulation and degrades others [*Liu et al.*, 2001]. It is not included in the present simulation.

[8] The ^{210}Pb source in the model assumes a uniform ^{222}Rn emission of 1.0 atom cm^{-2} s^{-1} from land under nonfreezing conditions. Following *Jacob and Prather* [1990], we reduce the flux by a factor of 3 under freezing conditions. Zero emission is assumed from oceans and ice-covered surfaces. The ^{7}Be source is taken from *Lal and Peters* [1967] as a function of altitude and latitude. About two thirds of the ^{7}Be is generated in the stratosphere and one third in the troposphere. The dependence of ^{7}Be production on season or longitude is small and is neglected here.

[9] Our initial simulation of ^{7}Be given by *Liu et al.* [2001] showed that the ^{7}Be cross-tropopause flux in the GEOS1 meteorological fields is too fast by a factor of 3–4, consistent with the excessive O_3 flux from the stratosphere found by *Bey et al.* [2001a]. We have since found the same problem in the GEOS3 fields. In the stratosphere, ^{7}Be concentrations are determined by a local balance between production and radioactive decay. We correct the excessive ^{7}Be flux from the stratosphere in our tropospheric simulations by scaling down globally the stratospheric ^{7}Be source [*Liu et al.*, 2001]. *Bey et al.* [2001a] found that although the magnitude of the cross-tropopause O_3 flux is too large, the latitudinal and seasonal variations of that flux are consistent with current knowledge [*Stohl et al.*, 2003]. Thus a uniform reduction in the ^{7}Be cross-tropopause flux should not induce large errors in the latitudinal or seasonal distribution of this flux. The reader is referred to *Liu et al.* [2001] for more discussion of this issue. For O_3 we circumvent the cross-tropopause flux problem by using the Synoz flux boundary condition [*McLinden et al.*, 2000], which imposes a cross-tropopause O_3 flux of 475 Tg yr^{-1}.

[10] After the correction for the cross-tropopause transport, we find that the model gives a good simulation of observed ^{210}Pb and ^{7}Be concentrations and deposition fluxes at surface sites worldwide with no systematic global bias, and that the observed latitudinal and seasonal distributions are successfully reproduced [*Liu et al.*, 2001]. PEM-West A and TRACE-P results were not presented by *Liu et al.* [2001] and therefore we will present some discussion here.

[11] The simulation of tropospheric O_3 in GEOS-CHEM uses a detailed representation of tropospheric O_3-NO_x-hydrocarbon chemistry [*Bey et al.*, 2001a]. The model solves the chemical evolution of 80 chemical species with a fast Gear solver [*Jacobson and Turco*, 1994]. The GEOS-CHEM versions used here (4.6 and 4.26) include an improved biomass burning emission inventory with seasonal variability constrained by satellite observations [*Duncan et al.*, 2003] but with no interannual variability. Biomass burning over continental Southeast Asia lasts from December to May and peaks in March. The TOMS aerosol index data suggest that biomass burning emissions in Southeast Asia in 1991 and 2001 were within 15% of the climatological average [*Heald et al.*, 2003].

[12] A global evaluation of the GEOS-CHEM simulation of tropospheric O_3-NO_x-hydrocarbon chemistry was presented by *Bey et al.* [2001a]. The model reproduces the climatological monthly mean O_3 concentrations in the ozonesonde record to within usually 10 parts per billion by volume (ppbv), and captures the phase of the seasonal cycle to within 1–2 months, although it underestimates the seasonal amplitude at northern midlatitudes. More specific evaluations of model results with O_3 observations in different regions of the world have been conducted for the western Pacific [*Bey et al.*, 2001b], the Asian Pacific Rim [*Liu et al.*, 2002], the Middle East [*Li et al.*, 2001], the United States [*Fiore et al.*, 2002a, 2002b, 2003a, 2003b], the North Atlantic [*Li et al.*, 2002a, 2002b], and the tropics [*Chandra et al.*, 2002; *Martin et al.*, 2002].

[13] Our O_3 simulations presented here focus on the periods of the aircraft missions but include an 18-month initialization for each period. To investigate source regions of O_3 in the model, we decompose O_3 (actually odd oxygen or O_x) into tagged tracers where tagging indicates different source regions [*Wang et al.*, 1998; *Fiore et al.*, 2002a; *Li et al.*, 2002a; *Liu et al.*, 2002]. In the tagged O_3 tracer simulation, we use daily mean 3-D fields of O_x production rates and loss frequencies archived from the standard full-chemistry simulation and transport five separate O_x tracers originating from different regions, i.e., the stratosphere, the upper troposphere (400 hPa-tropopause), the middle troposphere (700–400 hPa), the continental lower troposphere (surface-700 hPa), and the marine lower troposphere. The decomposition is linear so that summing the concentrations of all five tracers reproduces the results from the standard simulation.

[14] The radionuclide simulations presented here include a multi-year initialization starting with low concentrations of ^{222}Rn, ^{210}Pb and ^{7}Be. This long initialization is necessary to bring ^{210}Pb into steady state in the stratosphere.

3. Analysis of ^{210}Pb-^{7}Be-O_3 Relationships

[15] In this section we present a comparison of model results for ^{210}Pb, ^{7}Be, and O_3 with observations up to 12-km altitude from the three aircraft missions of Figure 1, and examine the constraints offered by ^{210}Pb-^{7}Be-O_3 relationships on the sources of O_3. The O_3 data are time averages over the 10–30 min sampling interval for the radionuclides. Model output is sampled every 3 hours along the flight tracks. Concentrations of ^{7}Be were below the detection limit (10 fCi SCM^{-1}) for 24%, 14%, and 33% of the samples from PEM-West A, PEM-West B, and TRACE-P, respectively. In those cases we assume a concentration of half the detection limit. Observations of ^{210}Pb were never below the detection limit (0.5 fCi SCM^{-1}).

[16] To describe the ^{210}Pb-^{7}Be-O_3 relationships, we calculate the lines of best fit using the reduced-major-axis (RMA) method [*Hirsch and Gilroy*, 1984]. Standard errors for the intercept and the slope are computed as described by *Miller and Kahn* [1962]. We also tried a chi-square fitting (or weighted least-squares fitting) technique [*Press et al.*, 1992] and find that it yields results generally consistent with those obtained from the RMA method.

3.1. PEM-West A

[17] This mission (September–October 1991) took place during the tail end of the summer monsoon season. We compare simulated and observed vertical distributions of ^{210}Pb, ^{7}Be, and O_3 concentrations over three regions (Figure 1) where intensive flights were flown. Following

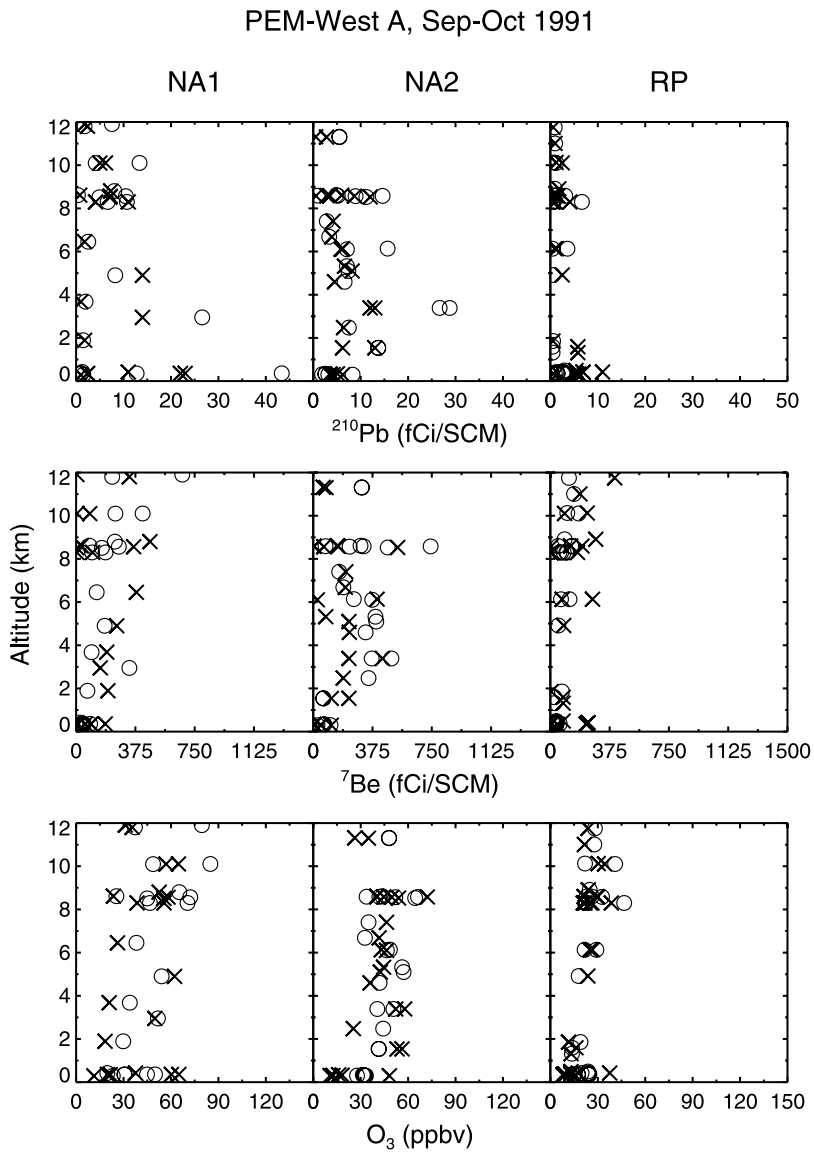

Figure 2. Comparison between simulated (open circles) and observed (crosses) vertical distributions of ^{210}Pb, ^{7}Be, and O_3 concentrations during PEM-West A for the three regions in Figure 1: near Asia (NA1 and NA2) and remote Pacific (RP). Model results are 3-hour instantaneous concentrations sampled along the flight tracks for the specific flight days and times.

Dibb et al. [1996], we call these regions "remote Pacific" (RP) and "near Asia" (NA1 and NA2). NA2 sampled northern midlatitudes outflow while NA1 and RP are subtropical or tropical. The comparisons are shown in Figure 2. The ^{210}Pb observations near Asia show much higher values than those over the remote Pacific, as would be expected. The vertical gradients of ^{210}Pb concentrations are generally weak and many samples in the free troposphere show higher concentrations than in the boundary layer, reflecting the role of convective transport during that season in lifting ^{222}Rn to the free troposphere. Observed concentrations for ^{7}Be are low relative to the typical 400–1000 fCi SCM^{-1} range observed in other regions [*Dibb et al.*, 1996], reflecting the general upwelling conditions and frequent rainfall of the summer monsoon as well as a seasonal minimum in transport from the stratosphere [*Stohl et al.*, 2003]. Simulated concentrations of ^{210}Pb and ^{7}Be are consistent with these patterns.

[18] The model reproduces the O_3 observations in PEM-West A with no systematic bias (Figure 2). Observed O_3 concentrations in the free troposphere near Asia are substantially (18 ppbv on average) higher than over the remote Pacific region, which may be largely explained by the lower latitude of the latter region where photochemical destruction exceeds production [*Davis et al.*, 1996].

[19] Figure 3 shows the simulated and observed relationships of O_3 with ^{210}Pb and ^{7}Be during PEM-West A for three altitude bins (0–3, 3–8, 8–12 km) near Asia and over the remote Pacific. The observations show a positive covariation of ^{210}Pb and O_3 at all altitudes near Asia [*Dibb et al.*, 1996] with the slope $\Delta O_3/\Delta^{210}$Pb ranging from 2.8 ± 0.3 to 4.3 ± 0.9 ppbv/fCi SCM^{-1}. Strong O_3-^{210}Pb correlation is also observed over the remote Pacific in the upper but not in the lower troposphere. The model reproduces these observed ^{210}Pb-O_3 relationships but tends to overestimate

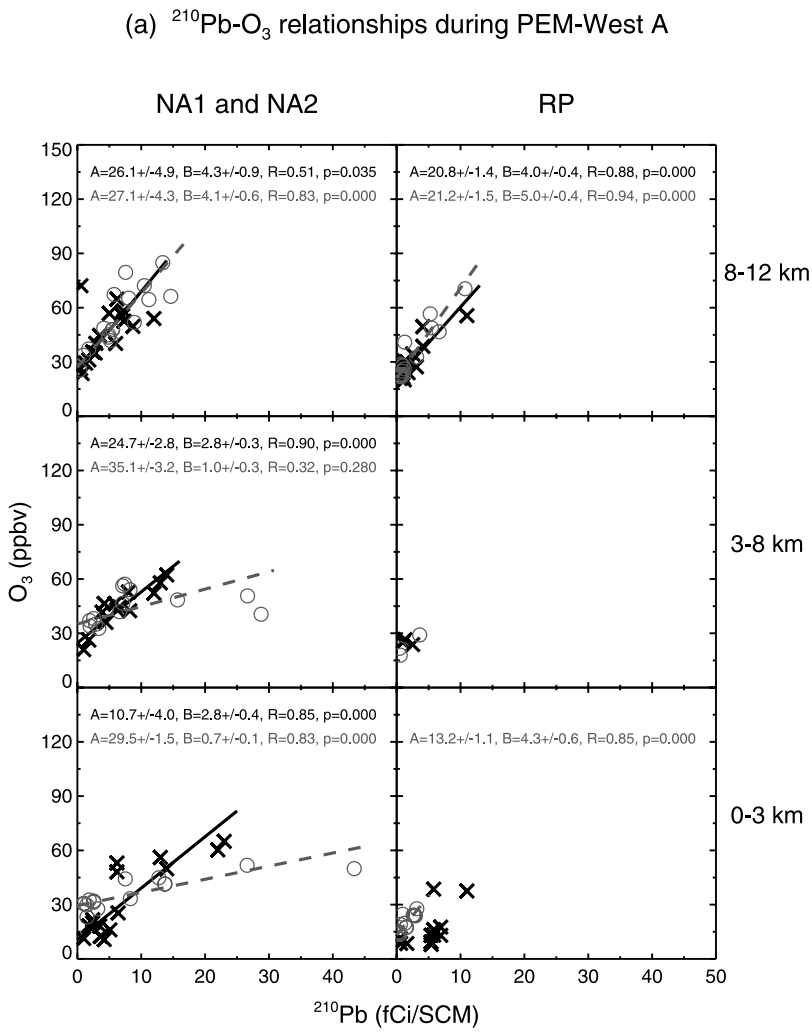

Figure 3. Scatterplots of O_3 against (a) ^{210}Pb and (b) ^{7}Be during PEM-West A in three altitude bins (0–3, 3–8, 8–12 km) near Asia (NA1 and NA2, left column) and over the remote Pacific (RP, right column), respectively. Model results (open circles and dashed lines) are compared with the observations (crosses and solid lines). The lines of best fit $[O_3] = A + B [^{210}Pb]$ and $[O_3] = A + B [^{7}Be]$ are calculated using the RMA method [*Hirsch and Gilroy*, 1984] if the Pearson correlation coefficient R is greater than 0.3. Inset of each panel are intercept A, slope B, R, and p values indicating the significance level of the linear correlation: $p < 0.01$ (highly significant), $0.01 < p < 0.05$ (significant), $0.05 \leq p < 0.10$ (almost significant), and $p \geq 0.10$ (not significant). Standard errors for A and B [*Miller and Kahn*, 1962] are also given. The model correlation results are shown in light gray and the observations in black.

(underestimate) the observed correlations in the upper troposphere (middle troposphere). It reproduces well the observed $\Delta O_3/\Delta^{210}$Pb values in the upper troposphere in both regions, implying a good simulation of deep convective outflow of O_3 from the Asian continent, as discussed below.

[20] The PEM-West A data show little correlation between the ^{7}Be and O_3 observations anywhere (Figure 3b) and the model overestimates the correlations in the upper troposphere. Even in the model, we find from the tagged tracer analysis that the stratosphere contributes less than 20% to upper tropospheric O_3 over the PEM-West A domain. We previously found that stratospheric O_3 accounts for only about 6–8 ppbv O_3 in the upper troposphere over Hong Kong during this season [*Liu et al.*, 2002].

[21] *Dibb et al.* [1996] hypothesized that frequent wet convection was the mechanism responsible for the ^{210}Pb-O_3 relationships observed in the free troposphere during PEM-West A. This hypothesis agrees with what is seen in our model. In late summer-early fall, we find that convection is the principal process transporting surface pollution (O_3 and its precursors) to the middle and upper troposphere, and this is followed by transport eastward to the western Pacific [*Liu et al.*, 2002]. During PEM-West A, the "near Asia" regions (Figure 1) are directly influenced by this convective outflow (Figure 4). Part of this outflow circulates around the western Pacific subtropical high, leading to positive ^{210}Pb-O_3 correlations in the upper troposphere over the remote Pacific.

3.2. PEM-West B

[22] We compare simulated and observed vertical distributions of ^{210}Pb, ^{7}Be, and O_3 concentrations in Figure 5,

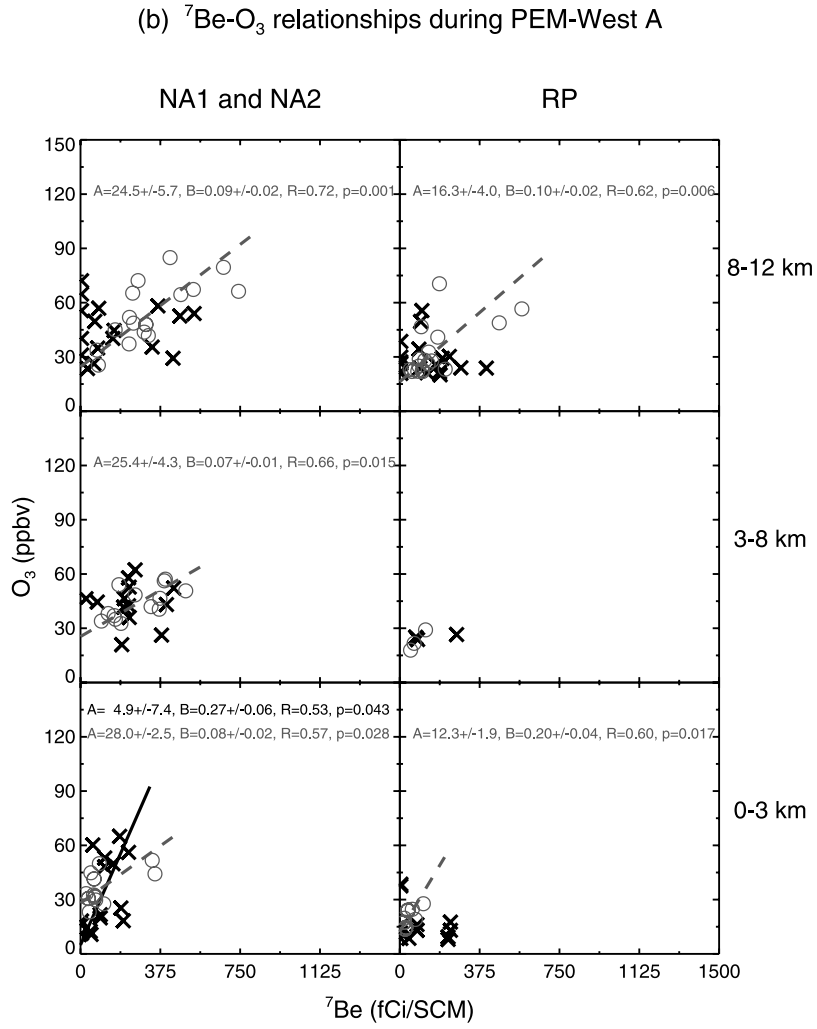

Figure 3. (continued)

for similar regions (Figure 1) as PEM-West A. The ^{210}Pb-^{7}Be-O_3 relationships are presented in Figure 6. The ^{210}Pb and ^{7}Be results were previously discussed by *Liu et al.* [2001]. While the PEM-West A ^{210}Pb concentrations show relatively weak vertical gradients, the PEM-West B ^{210}Pb observations indicate a decreasing trend with altitude near Asia, as the continental outflow is largely confined to the lower troposphere. The high ^{7}Be concentrations in some of the samples indicate stronger seasonal stratospheric influence than during PEM-West A. The model captures this influence and the contrasting behavior between the two missions. The model overestimates the ^{7}Be concentrations in the middle troposphere over the remote Pacific, but this appears to be due to insufficient aerosol scavenging rather than excessive stratospheric input [*Liu et al.*, 2001].

[23] *Bey et al.* [2001b] previously examined the Asian outflow of O_3 to the western Pacific during PEM-West B using an earlier version of GEOS-CHEM. Near Asia the substantial enhancement of O_3 during PEM-West B relative to PEM-West A reflects the stronger continental outflow and intrusion of stratospheric air into the upper troposphere in spring. Over the remote Pacific, O_3 values in the free troposphere are about twice as much of those in fall due to efficient net production of O_3 [*Crawford et al.*, 1997a]. The model reproduces these general patterns in the O_3 observations and shows no significant bias.

[24] O_3 and ^{210}Pb concentrations only weakly correlate near Asia either in the model or in the observations (Figure 6a). The observed ^{210}Pb-O_3 relationship in the upper troposphere near Asia shows two branches because of the latitudinal variation of O_3; ^{210}Pb and O_3 concentrations appear positively correlated at low latitudes but negatively correlated at midlatitudes (not shown). By contrast, ^{210}Pb and O_3 are correlated at all altitudes over the remote Pacific, with $\Delta O_3/\Delta^{210}$Pb ranging from 2.3 ± 0.6 to 9.2 ± 0.7 ppbv/fCi SCM^{-1} and increasing with altitude (Figure 6a). This reflects the slow but sustained rate of O_3 production in Asian outflow in that season [*Crawford et al.*, 1997b], as shown here in Figure 7. Strong production of O_3 in Southeast Asian boundary layer is due to seasonal biomass burning (Figure 7c). The remote Pacific domain, situated at lower latitudes than the near Asia domain, sampled a greater influence of biomass burning outflow exported to the Pacific in convection and warm conveyor belts (WCBs) [*Liu et al.*, 2003].

[25] The model shows strong O_3-^{7}Be correlations in the free troposphere, reflecting subsidence associated with the dry air stream of midlatitude cyclones [*Cooper et al.*, 2002]

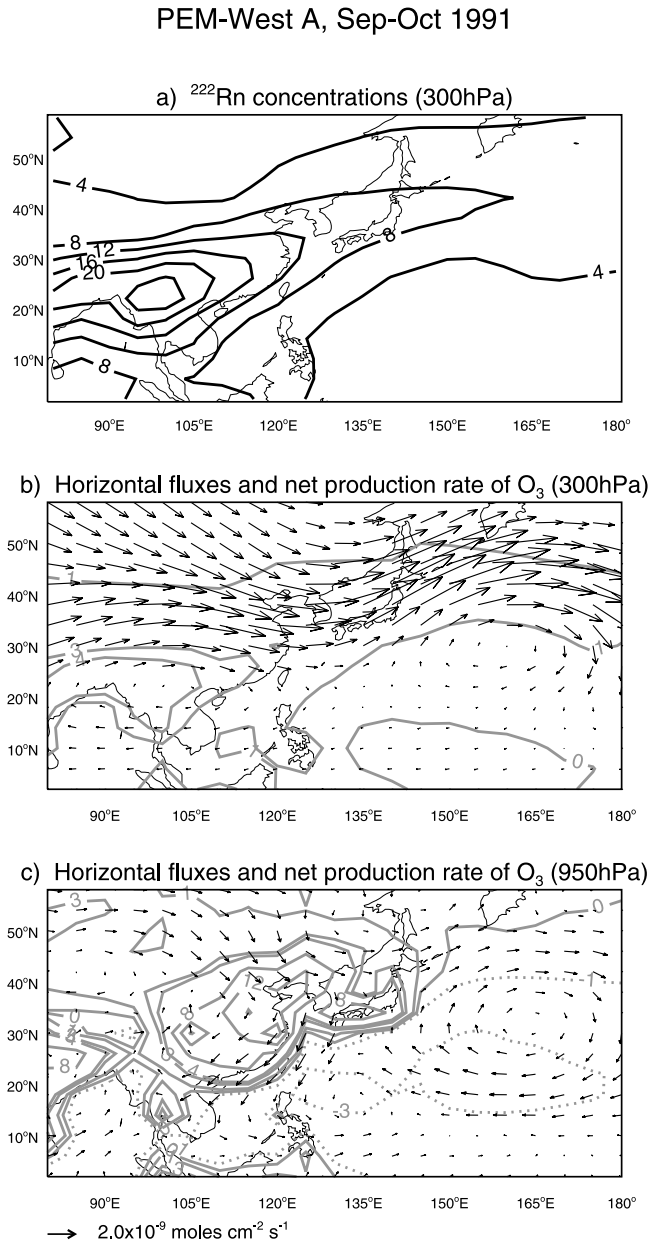

Figure 4. (a) Simulated mean ^{222}Rn concentrations (pCi SCM^{-1}; 1 pCi SCM^{-1} = 10^3 fCi SCM^{-1}) at 300 hPa for September–October 1991, indicative of frequent convection over the Asian continent. (b) Simulated mean horizontal fluxes (arrows, moles cm^{-2} s^{-1}) and net production rate (contours, ppbv day^{-1}) of O_3 at 300 hPa for September–October 1991. (c) Same as Figure 4b except for 950 hPa. Contour levels for ^{222}Rn concentrations are 4, 8, 12, 16, 20, 24. Contour levels for net production rate of O_3 are −3, −1, 0, 1, 3, 4, 8, 12, 16.

and the western Pacific subtropical High, but these correlations are not apparent in the observations perhaps because of complications from aerosol scavenging (Figure 6b). Tagged tracer simulations indicate that about 20% of model O_3 at 500 hPa originates from the stratosphere.

3.3. TRACE-P

[26] Most flights during TRACE-P were near Asia (Figure 1). We compare in Figure 8 the simulated and observed vertical distributions of ^{210}Pb, ^{7}Be and O_3 concentrations over the TRACE-P period for two regions separated at 30°N (see Figure 1). The ^{210}Pb-^{7}Be-O_3 relationships are presented in Figure 9. As during PEM-West B, the TRACE-P ^{210}Pb observations indicate a generally decreasing trend with altitude. The higher extreme values of ^{210}Pb in the boundary layer during TRACE-P are consistent with a stronger continental outflow than during PEM-West B [*Liu et al.*, 2003]. The ^{7}Be observations show larger variability, in particular in the middle and lower troposphere, than those for PEM-West B. The lack of vertical trend is partly due to the occurrence of high ^{7}Be values in the boundary layer, which we cannot reproduce in the model. The latter do not correlate with other indicators of subsidence and instead are mostly associated with Asian outflow (200–450 ppbv CO, 20–70 fCi SCM^{-1} ^{210}Pb); their source is unclear (J. E. Dibb, personal communication, 2003). They were not observed in PEM-West B (Figure 5).

[27] The observed O_3 concentrations generally do not correlate with ^{210}Pb concentrations north of 30°N (NA2 in Figure 9a). They are however correlated at all altitudes south of 30°N, with $\Delta O_3/\Delta^{210}$Pb increasing with altitude similarly to the remote Pacific data during PEM-West B (Figure 6a). Although TRACE-P was shifted ~3 weeks later in spring than PEM-West B and thus featured stronger photochemical production of O_3 [*Davis et al.*, 2003], the overall patterns for O_3 production and transport are similar (compare Figure 7 and Figure 10). As discussed earlier for PEM-West B, the WCB and convective export of effluents from Southeast Asian biomass burning dominates O_3 production and generates the positive ^{210}Pb-O_3 correlation observed and simulated in the low-latitude middle and upper troposphere. Boundary layer outflow behind cold fronts is associated with O_3 production (positive ^{210}Pb-O_3 correlation) south of 30°N but not further north. Similar to our results for PEM-West B, the model shows strong O_3-^{7}Be correlations that are not seen in the observations (Figure 9b) but are associated with only moderate stratospheric influence (30% of O_3 at 500 hPa north of 30°N).

4. Summary and Conclusions

[28] We have used a global 3-D model of tropospheric chemistry driven by assimilated meteorological data to analyze the observed ^{210}Pb-^{7}Be-O_3 relationships during three aircraft campaigns over the western Pacific: PEM-West A (September–October 1991), PEM-West B (February–March 1994), and TRACE-P (February–April 2001). The objective of this study was to examine the constraints offered by ^{210}Pb-^{7}Be-O_3 relationships on the sources of tropospheric O_3, with focus on Asian outflow to the Pacific.

[29] During PEM-West A, O_3 and ^{210}Pb concentrations are correlated at all altitudes near Asia, and in the upper troposphere only over the remote Pacific. In contrast, during PEM-West B and TRACE-P, the ^{210}Pb-O_3 correlations are strong in the low-latitude regions and over the remote Pacific, but are generally absent at midlatitudes near Asia. Our model analyses show that frequent wet convection in September–October (PEM-West A) and the shift of convection from China in late summer-early fall to Southeast Asia in spring (PEM-West B and TRACE-P) are responsible for this contrast. Boundary layer outflow behind cold fronts

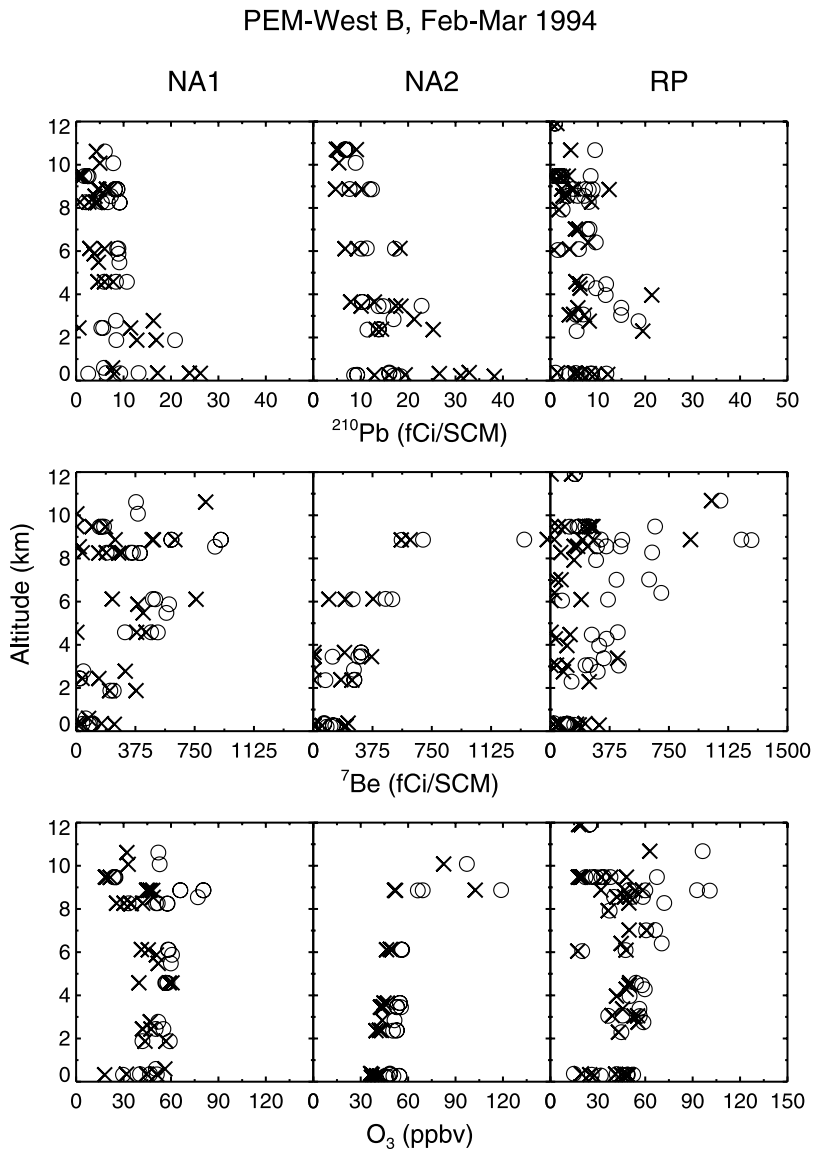

Figure 5. Comparison between simulated (open circles) and observed (crosses) vertical distributions of ^{210}Pb, ^{7}Be, and O_3 concentrations during PEM-West B for the three regions in Figure 1: near Asia (NA1 and NA2) and the remote Pacific (RP). Model results are 3-hour instantaneous concentrations sampled along the flight track for the specific flight days and time. Stratospheric data above 8 km (^{7}Be > 1500 fCi SCM^{-1} and O_3 > 150 ppbv) are not shown.

and sustained slow net O_3 production over the western Pacific during spring eventually leads to a positive ^{210}Pb-O_3 correlation in air masses sampled in the boundary layer over the remote Pacific far downwind of the Asian continent. Seasonal biomass burning over Southeast Asia in spring is responsible for the positive ^{210}Pb-O_3 correlations in the middle and upper troposphere at low latitudes.

[30] During PEM-West A, no ^{7}Be-O_3 correlations are found either near Asia or over the remote Pacific owing to weak stratospheric influence. During PEM-West B and TRACE-P, the model shows much stronger ^{7}Be-O_3 correlations than the observations, even though the stratospheric influence on O_3 in the model is rather modest (20–30% of total O_3 at northern midlatitudes at 500 hPa). This result implies that the model at least does not underestimate the stratospheric contribution to the observed springtime maximum in O_3 at northern midlatitudes. We have argued previously that this maximum is mostly the result of anthropogenic pollution [*Wang et al.*, 1998; *Li et al.*, 2002a].

[31] Overall, our results show that a global 3-D model interpretation of observed ^{210}Pb-^{7}Be-O_3 correlations provides an important test of our understanding of the factors controlling tropospheric ozone. Our simulated ^{210}Pb-O_3 and ^{7}Be-O_3 correlations tend to be stronger than observed, presumably because of fewer factors of variability in the model. The stronger ^{7}Be-O_3 correlations in the model could also be due to overestimate of subsidence. Fine-resolution models with more complete and detailed physical and chemical processes should produce larger variability and have potential to improve the simulation. Better knowledge of the ^{222}Rn source distribution (assumed here to be

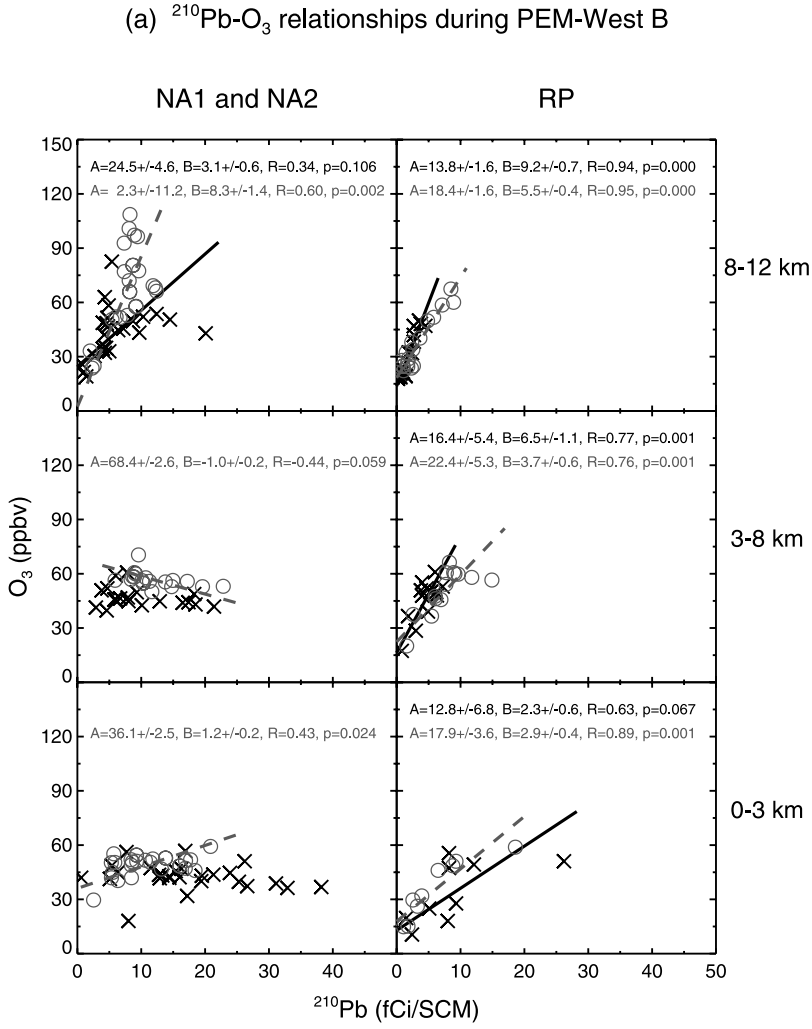

Figure 6. Scatterplots of O_3 against (a) ^{210}Pb and (b) ^{7}Be during PEM-West B in three altitude bins (0–3, 3–8, 8–12 km) over near Asia (NA1 and NA2, left column) and over the remote Pacific (RP, right column), respectively. Model results (open circles and dashed lines) are compared with the observations (crosses and solid lines). Upper tropospheric samples with ^{7}Be > 1500 fCi SCM^{-1} or O_3 > 100 ppbv are not used. The lines of best fit are calculated by the RMA method if the Pearson correlation coefficient R is greater than 0.3. See caption of Figure 3 for details.

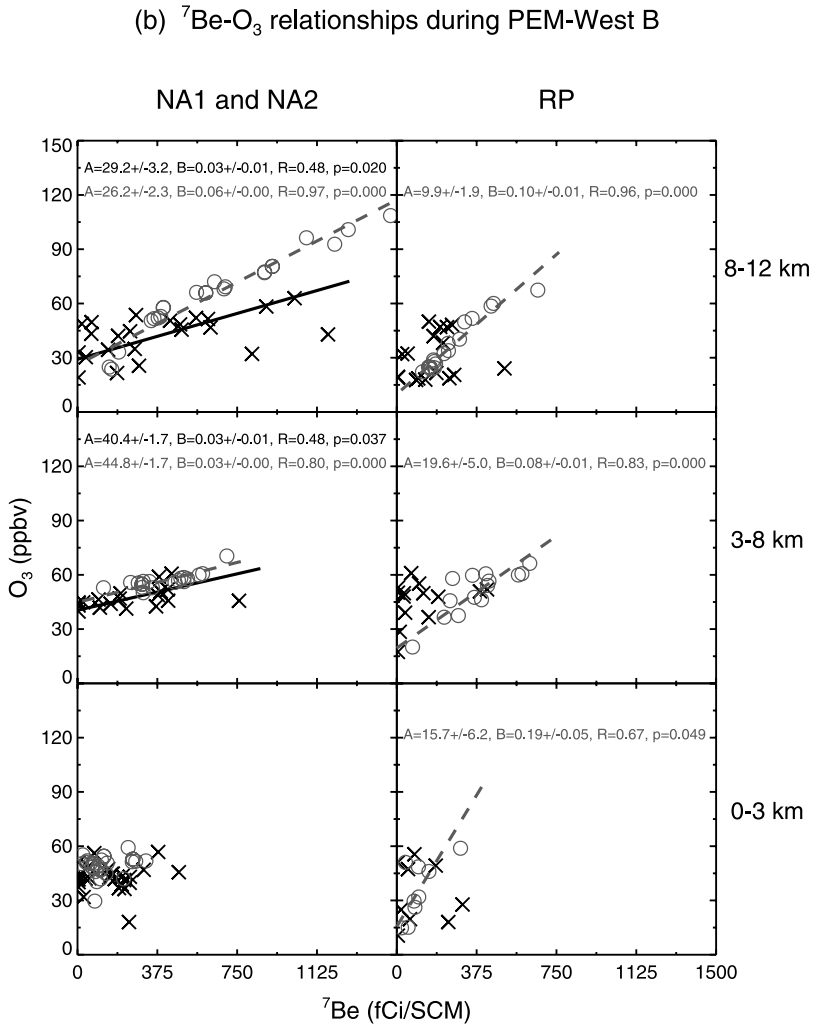

Figure 6. (continued)

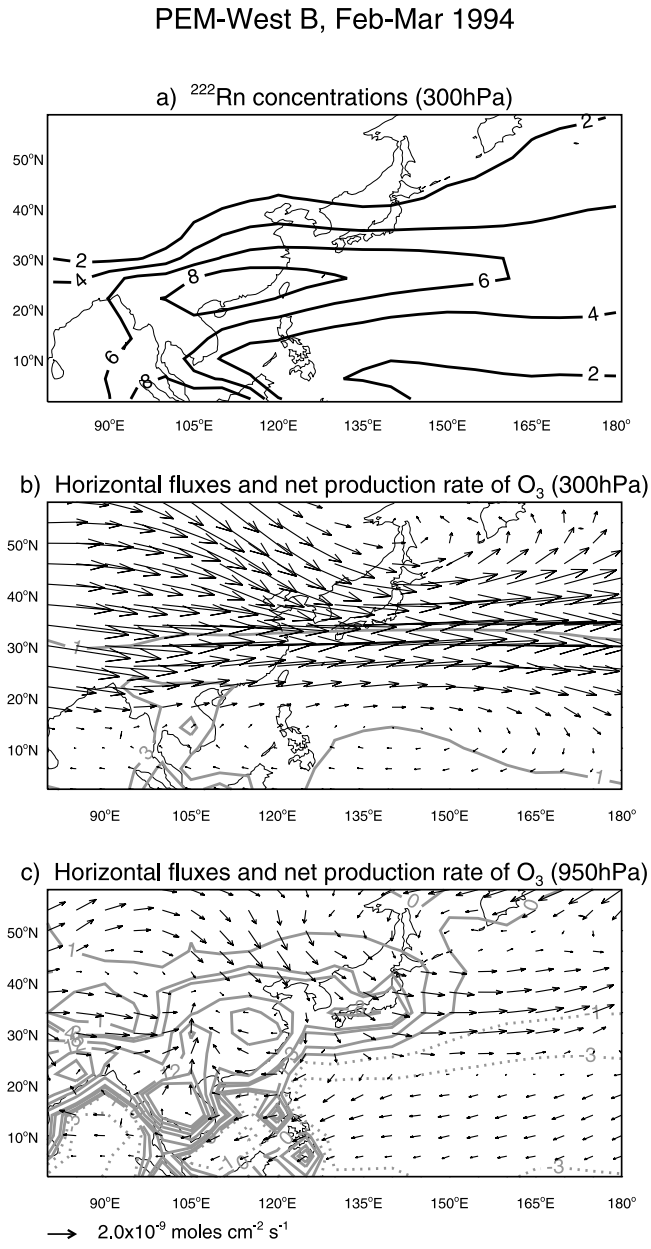

Figure 7. (a) Simulated mean ^{222}Rn concentrations (pCi SCM^{-1}) at 300 hPa for February–March 1994, indicative of frequent convection over Southeast Asia. (b) Simulated mean horizontal fluxes (arrows, moles cm^{-2} s^{-1}) and net production rate (contours, ppbv day^{-1}) of O_3 at 300 hPa for February–March 1994. (c) Same as Figure 7b except for 950 hPa. Contour levels for ^{222}Rn concentrations are 2, 4, 6, 8, 10. Contour levels for net production rate of O_3 are −3, −1, 0, 1, 3, 4, 8, 12, 16, 20.

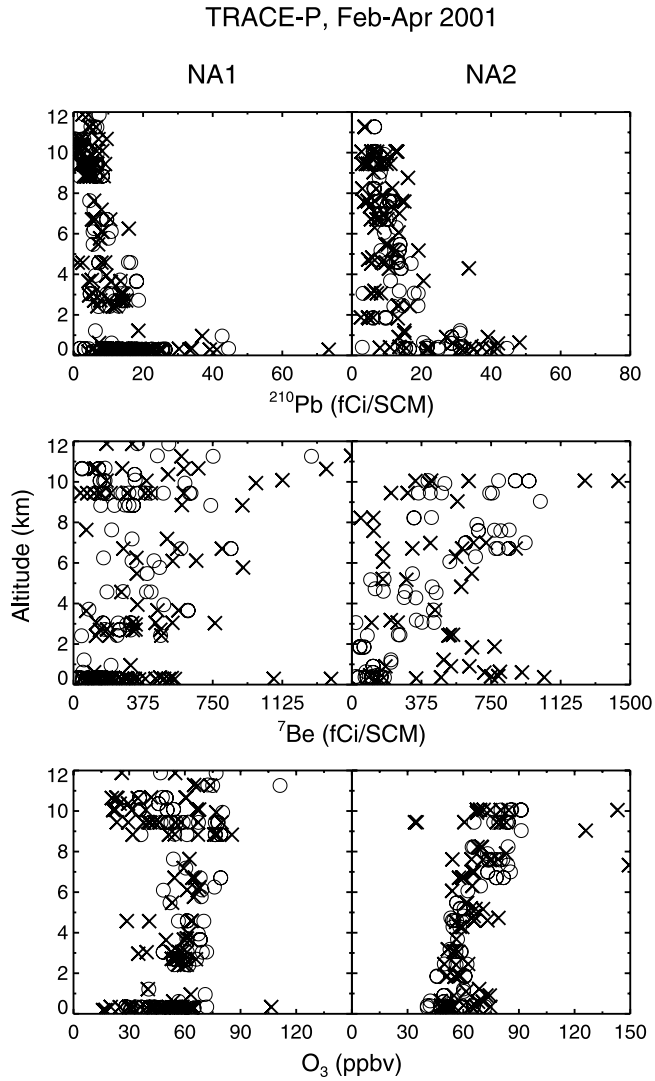

Figure 8. Comparison between simulated (open circles) and observed (crosses) vertical distributions of ^{210}Pb, ^{7}Be and O_3 concentrations during TRACE-P for the two regions in Figure 1: NA1 and NA2. Model results are 3-hour instantaneous concentrations sampled along the flight track for the specific flight days and time. Stratospheric data (^{7}Be > 1500 fCi SCM^{-1} and O_3 > 150 ppbv) are not shown.

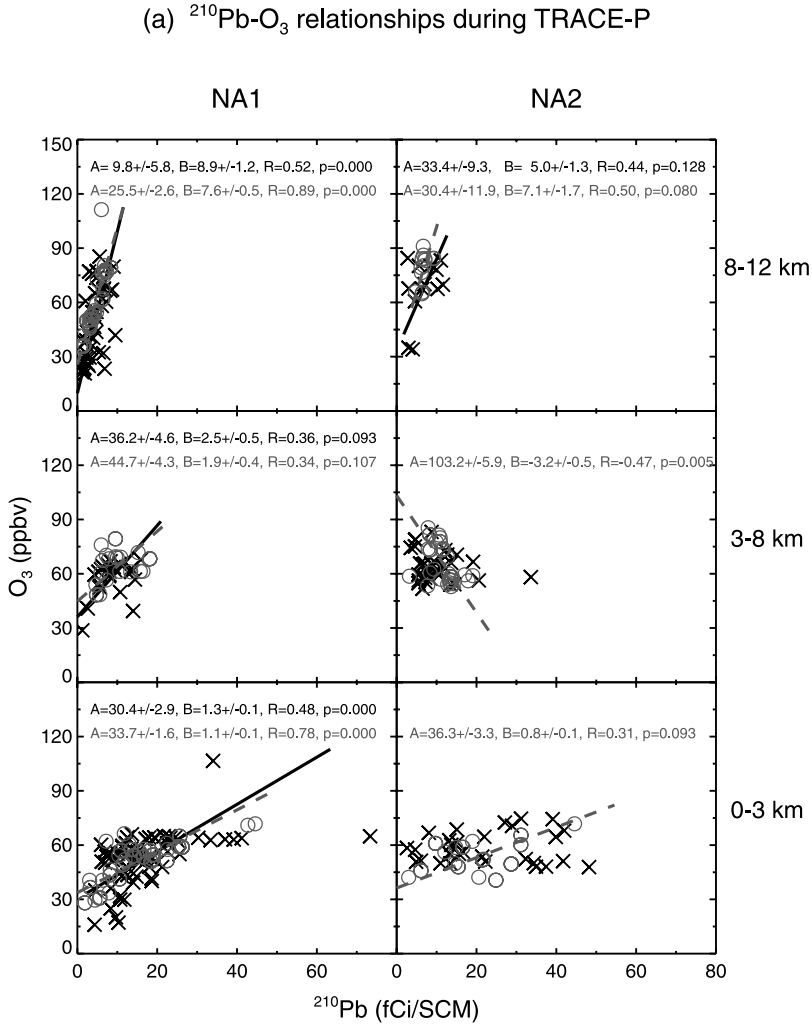

Figure 9. Scatterplots of O_3 against (a) ^{210}Pb and (b) ^{7}Be during TRACE-P in three altitude bins (0–3, 3–8, 8–12 km) over near Asia (NA1, left column; and NA2, right column). See Figure 1 for the definitions of NA1 and NA2. Model results (open circles and dashed lines) are compared with the observations (crosses and solid lines). Samples with ^{7}Be > 1500 fCi SCM^{-1} or O_3 > 100 ppbv are not used, except one highly polluted air mass sample (106.6 ppbv O_3, 34 fCi/SCM^{-1} ^{210}Pb, and below-detection-limit ^{7}Be) in the 0–3 km altitude bin (NA1). The lines of best fit are calculated by the RMA method if the Pearson correlation coefficient R is greater than 0.3. See caption of Figure 3 for details.

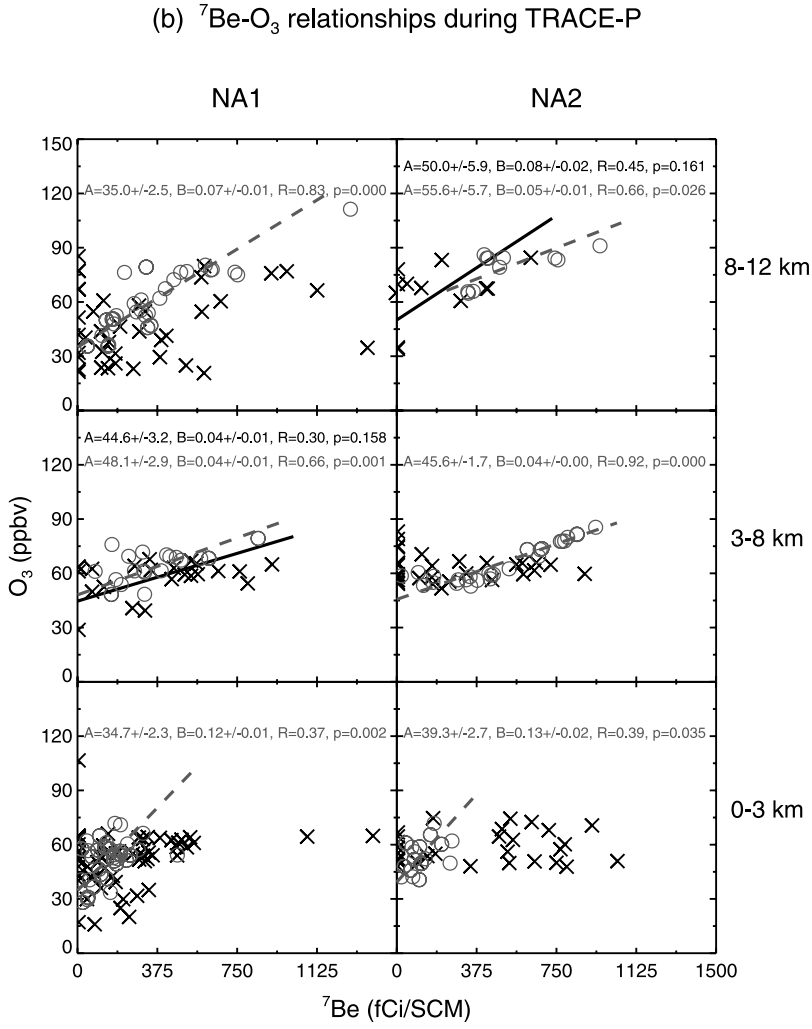

Figure 9. (continued)

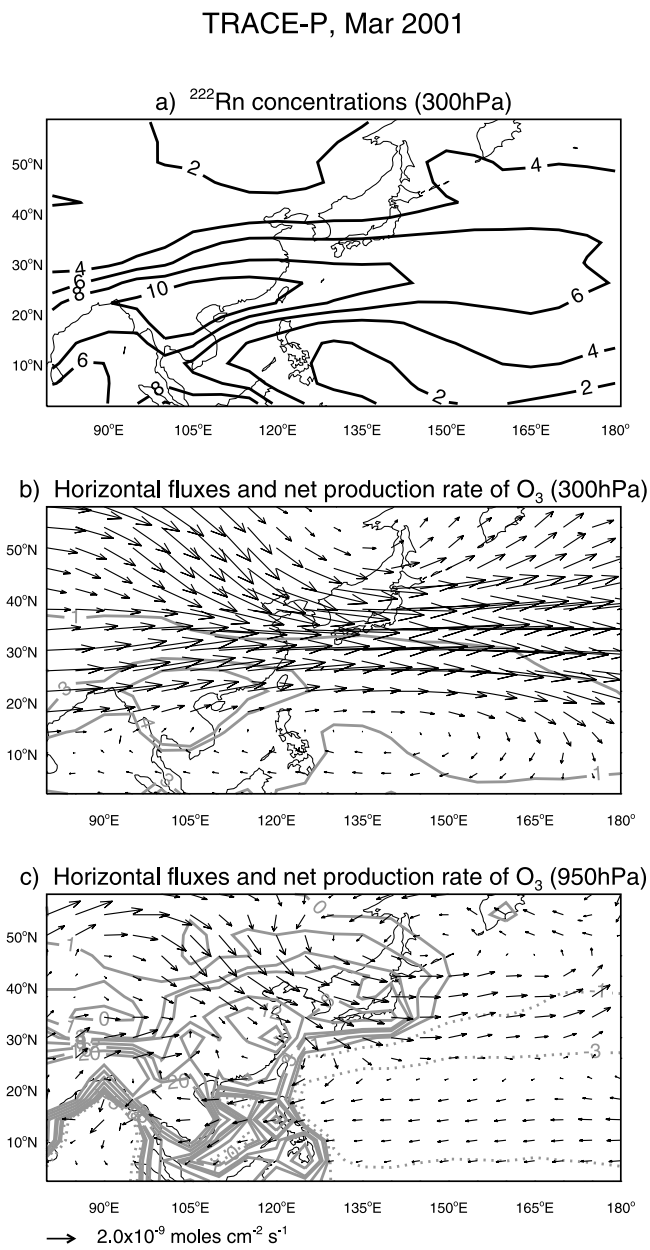

Figure 10. (a) Simulated mean ^{222}Rn concentrations (pCi SCM^{-1}) at 300 hPa for March 2001, indicative of frequent convection over Southeast Asia. (b) Simulated monthly mean horizontal fluxes (arrows, moles cm^{-2} s^{-1}) and net production rate (contours, ppbv day^{-1}) of O_3 at 300 hPa for March 2001. (c) Same as Figure 10b except for 950 hPa. Contour levels for ^{222}Rn concentrations are 2, 4, 6, 8, 10. Contour levels for net production rate of O_3 are −3, −1, 0, 1, 3, 4, 8, 12, 16, 20.

uniform over land) would strengthen the constraints from the observed ^{210}Pb-O_3 correlations.

[32] **Acknowledgments.** This research was funded by the NASA Atmospheric Chemistry Modeling and Analysis Program (ACMAP). HL is grateful to Jim H. Crawford for the generous support of his activities at the National Institute of Aerospace. We thank Steven C. Wofsy for his helpful comments.

References

Allen, D. J., R. B. Rood, A. M. Thompson, and R. D. Hudson (1996), Three-dimensional radon 222 calculations using assimilated meteorological data and a convective mixing algorithm, *J. Geophys. Res.*, *101*, 6871–6881.

Balkanski, Y. J., D. J. Jacob, G. M. Gardner, W. C. Graustein, and K. K. Turekian (1993), Transport and residence times of tropospheric aerosols inferred from a global three-dimensional simulation of ^{210}Pb, *J. Geophys. Res.*, *98*, 20,573–20,586.

Bell, N., L. Hsu, D. J. Jacob, M. G. Schultz, D. R. Blake, J. H. Butler, D. B. King, J. M. Lobert, and E. Maier-Reimer (2002), Methyl iodide: Atmospheric budget and use as a tracer of marine convection in global models, *J. Geophys. Res.*, *107*(D17), 4340, doi:10.1029/2001JD001151.

Bey, I., D. J. Jacob, R. M. Yantosca, J. A. Logan, B. Field, A. M. Fiore, Q. Li, H. Liu, L. J. Mickley, and M. Schultz (2001a), Global modeling of tropospheric chemistry with assimilated meteorology: Model description and evaluation, *J. Geophys. Res.*, *106*, 23,073–23,096.

Bey, I., D. J. Jacob, J. A. Logan, and R. M. Yantosca (2001b), Asian chemical outflow to the Pacific in spring: Origins, pathways, and budgets, *J. Geophys. Res.*, *106*, 23,097–23,114.

Chandra, S., J. R. Ziemke, P. K. Bhartia, and R. V. Martin (2002), Tropical tropospheric ozone: Implications for dynamics and biomass burning, *J. Geophys. Res.*, *107*(D14), 4188, doi:10.1029/2001JD000447.

Cooper, O. R., J. L. Moody, D. D. Parrish, M. Trainer, T. B. Ryerson, J. S. Holloway, G. Hübler, F. C. Fehsenfeld, and M. J. Evans (2002), Trace gas composition of midlatitude cyclones over the western North Atlantic Ocean: A conceptual model, *J. Geophys. Res.*, *107*(D7), 4056, doi:10.1029/2001JD000901.

Crawford, J. H., et al. (1997a), Implications of large scale shifts in tropospheric NOx levels in the remote tropical Pacific, *J. Geophys. Res.*, *102*, 28,447–28,468.

Crawford, J. H., et al. (1997b), An assessment of ozone photochemistry in the extratropical western North Pacific. Impact of continental outflow during the late winter/early spring, *J. Geophys. Res.*, *102*, 28,469–28,487.

Davis, D. D., et al. (1996), Assessment of ozone photochemistry in the western North Pacific as inferred from PEM-West A observations during the fall 1991, *J. Geophys. Res.*, *101*, 2111–2134.

Davis, D. D., et al. (2003), An assessment of western North Pacific ozone photochemistry based on springtime observations from NASA's PEM-West B (1994) and TRACE-P (2001) field studies, *J. Geophys. Res.*, *108*(D21), 8829, doi:10.1029/2002JD003232.

Dibb, J. E., R. W. Talbot, and G. L. Gregory (1992), Beryllium 7 and lead 210 in the western hemisphere Arctic atmosphere: Observations from three recent aircraft-based sampling programs, *J. Geophys. Res.*, *97*, 16,709–16,715.

Dibb, J. E., L. D. Meeker, R. C. Finkel, J. R. Southon, M. W. Caffee, and L. A. Barrie (1994), Estimation of stratospheric input to the Arctic troposphere: ^{7}Be and ^{10}Be in aerosols at Alert, Canada, *J. Geophys. Res.*, *99*, 12,855–12,864.

Dibb, J. E., R. W. Talbot, K. I. Klemm, G. L. Gregory, H. B. Singh, J. D. Bradshaw, and S. T. Sandholm (1996), Asian influence over the western North Pacific during the fall season: Inferences from lead 210, soluble ionic species and ozone, *J. Geophys. Res.*, *101*, 1779–1792.

Dibb, J. E., R. W. Talbot, B. L. Lefer, E. Scheuer, G. L. Gregory, E. V. Browell, J. D. Bradshaw, S. T. Sandholm, and H. B. Singh (1997), Distributionsof beryllium 7 and lead 210, and soluble aerosol-associated ionic species over the western Pacific: PEM-West B, February–March 1994, *J. Geophys. Res.*, *102*, 28,287–28,302.

Dibb, J. E., R. W. Talbot, E. M. Scheuer, G. Seid, M. A. Avery, and H. B. Singh (2003), Aerosol chemical composition in Asian continental outflow during the TRACE-P campaign: Comparison with PEM-West B, *J. Geophys. Res.*, *108*(D21), 8815, doi:10.1029/2002JD003111.

Duncan, B. N., R. V. Martin, A. C. Staudt, R. Yevich, and J. A. Logan (2003), Interannual and seasonal variability of biomass burning emissions constrained by satellite observations, *J. Geophys. Res.*, *108*(D2), 4100, doi:10.1029/2002JD002378.

Ehhalt, D., and M. Prather (2001), Atmospheric chemistry and greenhouse gases, in *Climate Change 2001: The Scientific Basis: Contribution of Working Group I to the Third Assessment Report of the Intergovernmental Panel on Climate Change*, pp. 239–287, Cambridge Univ. Press, New York.

Feely, H. W., R. J. Larsen, and C. G. Sanderson (1989), Factors that cause seasonal variations in beryllium-7 concentrations in surface air, *J. Environ. Radioact.*, *9*, 223–249.

Fiore, A. M., D. J. Jacob, I. Bey, R. M. Yantosca, B. D. Field, A. C. Fusco, and J. G. Wilkinson (2002a), Background ozone over the United States in summer: Origin, trend, and contribution to pollution episodes, *J. Geophys. Res.*, *107*(D15), 4275, doi:10.1029/2001JD000982.

Fiore, A. M., D. J. Jacob, B. D. Field, D. G. Streets, S. D. Fernandes, and C. Jang (2002b), Linking ozone pollution and climate change: The case

for controlling methane, *Geophys. Res. Lett.*, *29*(19), 1919, doi:10.1029/2002GL015601.

Fiore, A. M., D. J. Jacob, R. Mathur, and R. V. Martin (2003a), Application of empirical orthogonal functions to evaluate ozone simulations with regional and global models, *J. Geophys. Res.*, *108*(D14), 4431, doi:10.1029/2002JD003151.

Fiore, A., D. J. Jacob, H. Liu, R. M. Yantosca, T. D. Fairlie, and Q. Li (2003b), Variability in surface ozone background over the United States: Implications for air quality policy, *J. Geophys. Res.*, *108*(D24), 4787, doi:10.1029/2003JD003855.

Heald, C. L., D. J. Jacob, P. I. Palmer, M. J. Evans, G. W. Sachse, H. B. Singh, and D. R. Blake (2003), Biomass burning emission inventory with daily resolution: Application to aircraft observations of Asian outflow, *J. Geophys. Res.*, *108*(D21), 8811, doi:10.1029/2002JD003082.

Hirsch, R. M., and E. J. Gilroy (1984), Methods of fitting a straight line to data. Examples in water resources, *Water Resour. Bull.*, *20*, 705–711.

Hoell, J. M., D. D. Davis, S. C. Liu, R. E. Newell, M. Shipham, H. Akimoto, R. J. McNeal, R. J. Bendura, and J. W. Drewry (1996), Pacific Explortory Mission-West A (PEM-West A), September–October 1991, *J. Geophys. Res.*, *101*, 1641–1653.

Hoell, J. M., D. D. Davis, S. C. Liu, R. E. Newell, H. Akimoto, R. J. McNeal, and R. J. Bendura (1997), The Pacific Exploratory Mission-West Phase B: February–March 1994, *J. Geophys. Res.*, *102*, 28,223–28,240.

Jacob, D. J., and M. J. Prather (1990), Radon-222 as a test of boundary layer convection in a general circulation model, *Tellus*, *Ser. A*, *42*, 118–134.

Jacob, D. J., J. H. Crawford, M. M. Kleb, V. S. Connors, R. J. Bendura, J. L. Raper, G. W. Sachse, J. C. Gille, L. Emmons, and C. L. Heald (2003), Transport and Chemical Evolution over the Pacific (TRACE-P) aircraft mission: Design, execution, and first results, *J. Geophys. Res.*, *108*(D20), 9000, doi:10.1029/2002JD003276.

Jacobson, M. Z., and R. P. Turco (1994), A sparse-matrix, vectorized GEAR code for atmospheric transport models, *Atmos. Environ.*, *33*, 273–284.

Johnson, W. B., and W. Viezee (1981), Stratospheric ozone in the lower troposphere-I. Presentation and interpretation of aircraft measurements, *Atmos. Environ.*, *15*, 1309–1323.

Koch, D. M., D. J. Jacob, and W. C. Graustein (1996), Vertical transport of tropospheric aerosols as indicated by ^{7}Be and ^{210}Pb in a chemical tracer model, *J. Geophys. Res.*, *101*, 18,651–18,666.

Lal, D., and B. Peters (1967), Cosmic ray produced radioactivity on the Earth, in *Handbuch der Physik*, 46/2, edited by K. Sitte, pp. 551–612, Springer-Verlag, New York.

Lawrence, M. G., and P. J. Crutzen (1998), The impact of cloud particle gravitational settling on soluble trace gas distributions, *Tellus*, *Ser. B*, *50*, 263–289.

Li, Q., et al. (2001), A tropospheric ozone maximum over the Middle East, *Geophys. Res. Lett.*, *28*, 3235–3238.

Li, Q., D. J. Jacob, T. D. Fairlie, H. Liu, R. V. Martin, and R. M. Yantosca (2002a), Stratospheric versus pollution influences on ozone at Bermuda: Reconciling past analyses, *J. Geophys. Res.*, *107*(D22), 4611, doi:10.1029/2002JD002138.

Li, Q., et al. (2002b), Transatlantic transport of pollution and its effects on surface ozone in Europe and North America, *J. Geophys. Res.*, *107*(D13), 4166, doi:10.1029/2001JD001422.

Lin, S.-J., and R. B. Rood (1996), Multidimensional flux-form semi-Lagrangian transport schemes, *Mon. Weather Rev.*, *124*, 2046–2070.

Liu, H., D. J. Jacob, I. Bey, and R. M. Yantosca (2001), Constraints from ^{210}Pb and ^{7}Be on wet deposition and transport in a global three-dimensional chemical tracer model driven by assimilated meteorological fields, *J. Geophys. Res.*, *106*, 12,109–12,128.

Liu, H., D. J. Jacob, L. Y. Chan, S. J. Oltmans, I. Bey, R. M. Yantosca, J. M. Harris, B. N. Duncan, and R. V. Martin (2002), Sources of tropospheric ozone along the Asian Pacific Rim: An analysis of ozonesonde observations, *J. Geophys. Res.*, *107*(D21), 4573, doi:10.1029/2001JD002005.

Liu, H., D. J. Jacob, I. Bey, R. M. Yantosca, B. N. Duncan, and G. W. Sachse (2003), Transport pathways for Asian pollution outflow over the Pacific: Interannual and seasonal variations, *J. Geophys. Res.*, *108*(D20), 8786, doi:10.1029/2002JD003102.

Martin, R. V., et al. (2002), Interpretation of TOMS observations of tropical tropospheric ozone with a global model and in situ observations, *J. Geophys. Res.*, *107*(D18), 4351, doi:10.1029/2001JD001480.

McLinden, C. A., S. C. Olsen, B. Hannegan, O. Wild, M. J. Prather, and J. Sundet (2000), Stratospheric ozone in 3-D models: A simple chemistry and the cross-tropopause flux, *J. Geophys. Res.*, *105*, 14,653–14,665.

Miller, R. L., and J. S. Kahn (1962), *Statistical Analysis in the Geological Sciences*, pp. 204–210, John Wiley, Hoboken, N. J.

Moody, J. L., S. J. Oltmans, H. Levy II, and J. T. Merrill (1995), Transport climatology of tropospheric ozone, Bermuda, 1988–1991, *J. Geophys. Res.*, *100*, 7179–7194.

Press, W. H., S. A. Teukolsky, W. T. Vetterling, and B. P. Flannery (1992), *Numerical Recipes in FORTRAN 77*, vol. 1, *The Art of Scientific Computing*, Fortran Numer. Recipes, pp. 660–664, Cambridge Univ. Press, New York.

Prospero, J. M., R. Schmitt, E. Cuevas, D. L. Savoie, W. C. Graustein, K. K. Turekian, A. Volz-Thomas, A. Diaz, S. J. Oltmans, and H. Levy II (1995), Temporal variability of summer-time ozone and aerosols in the free troposphere over the eastern North Atlantic, *Geophys. Res. Lett.*, *22*, 2925–2928.

Reiter, R., K. Munzert, H.-J. Kanter, and K. Potzl (1983), Cosmogenic radionuclides and ozone at a mountain station at 3.0 km a. s. l., *Arch. Meteorol. Geophys. Bioklimatol.*, *Ser. B*, *32*, 131–160.

Stohl, A., et al. (2003), Stratosphere-troposphere exchange: A review, and what we have learned from STACCATO, *J. Geophys. Res.*, *108*(D12), 8516, doi:10.1029/2002JD002490.

Thompson, A. M. (1992), The oxidizing capacity of the Earth's atmosphere. Probable past and future changes, *Science*, *256*, 1157–1165.

Tsutsumi, Y., Y. Igarashi, Y. Zaizen, and Y. Makino (1998), Case studies of tropospheric ozone events observed at the summit of Mount Fuji, *J. Geophys. Res.*, *103*, 16,935–16,951.

Turekian, K. K., Y. Nozaki, and L. K. Benninger (1977), Geochemistry of atmospheric radon and radon products, *Annu. Rev. Earth Planet. Sci.*, *5*, 227–255.

Viezee, W., and H. B. Singh (1980), The distribution of beryllium-7 in the troposphere. Implications on stratosphere/tropospheric air exchange, *Geophys. Res. Lett.*, *7*, 805–808.

Wang, Y., D. J. Jacob, and J. A. Logan (1998), Global simulation of tropospheric O_3-NO_x-hydrocarbon chemistry: 3. Origin of tropospheric ozone and effects of non-methane hydrocarbons, *J. Geophys. Res.*, *103*, 10,757–10,768.

Wesely, M. L., and B. B. Hicks (1977), Some factors that affect the deposition rates of sulfur dioxide and similar gases on vegetation, *J. Air Pollut. Contr. Assoc.*, *27*, 1110–1116.

J. E. Dibb, Institute for the Study of Earth, Oceans, and Space, University of New Hampshire, 39 College Road, Morse Hall, Durham, NH 03824, USA.

A. M. Fiore, Program of Atmospheric and Oceanic Sciences, Princeton University, Princeton, NJ 08544, USA.

D. J. Jacob and R. M. Yantosca, Department of Earth and Planetary Sciences, Harvard University, Pierce Hall, 29 Oxford Street, Cambridge, MA 02138, USA. (djj@io.harvard.edu)

H. Liu, National Institute of Aerospace, 144 Research Drive, Hampton, VA 23666, USA. (hyl@post.harvard.edu)